

AD-A262 814



IDENTIFICATION PAGE

Form Approved  
OMB No. 0704-0188

1

page 1 hour per response, including the time for reviewing instructions, searching existing data sources, gathering and information. Send comments regarding this burden estimate or any other aspect of this collection of information, including Directorate for Information Operations and Reports, 1215 Jefferson Davis Highway, Suite 1204, Arlington, VA 22202-4302 and to the Office of Management and Budget, Paperwork Reduction Project (0704-0188), Washington, DC 20503

1. AGENCY USE ONLY (Leave blank)	2. REPORT DATE February 1993	3. REPORT TYPE AND DATES COVERED professional paper
4. TITLE AND SUBTITLE FEEDBACK CONTROL OF KARMAN VORTEX SHEDDING		5. FUNDING NUMBERS PR: HM40 PE: 0605861N WU: DN300051
6. AUTHOR(S) D. S. Park, D. M. Ladd, and E. W. Hendricks		
7. PERFORMING ORGANIZATION NAME(S) AND ADDRESS(ES) Naval Command, Control and Ocean Surveillance Center (NCCOSC) RDT&E Division San Diego, CA 92152-5001		8. PERFORMING ORGANIZATION REPORT NUMBER
9. SPONSORING/MONITORING AGENCY NAME(S) AND ADDRESS(ES) Office of Naval Research 800 N. Quincy Street Arlington, VA 22217		10. SPONSORING/MONITORING AGENCY REPORT NUMBER
11. SUPPLEMENTARY NOTES		
12a. DISTRIBUTION/AVAILABILITY STATEMENT  Authorized for public release; distribution is unlimited.		12b. DISTRIBUTION CODE

DTIC  
SELECT  
APR 12 1993  
S B D

13. ABSTRACT (Maximum 200 words)

A direct numerical simulation of the Navier-Stokes equations of a feedback controlled cylinder wake flow at the Reynolds number of 60 is presented. The simulation shows that vortex shedding behind a circular cylinder is suppressed to a significant degree by applying a feedback forcing with an appropriate phase via blowing/suction slots located at  $\pm 110^\circ$  from the leading edge. Depending on the phase of the feedback forcing relative to the vortex shedding phase, the shedding of the vortices is either suppressed (stabilized) or further enhanced (destabilized).

93 4 09 04

93-07498

8PO

Published in DSC-Vol. 38, Active Control of Noise and Vibration, ASME 1992.

14. SUBJECT TERMS active control torpedo		15. NUMBER OF PAGES	
		16. PRICE CODE	
17. SECURITY CLASSIFICATION OF REPORT UNCLASSIFIED	18. SECURITY CLASSIFICATION OF THIS PAGE UNCLASSIFIED	19. SECURITY CLASSIFICATION OF ABSTRACT UNCLASSIFIED	20. LIMITATION OF ABSTRACT SAME AS REPORT

UNCLASSIFIED

21a. NAME OF RESPONSIBLE INDIVIDUAL D. M. Ladd	21b. TELEPHONE (Include Area Code) (619) 553-1617	21c. OFFICE SYMBOL Code 574

DTIC QUALITY INSPECTED 4

<b>Accession For</b>	
NTIS GRA&I	<input checked="" type="checkbox"/>
DTIC TAB	<input type="checkbox"/>
Unannounced	<input type="checkbox"/>
Justification	
By _____	
Distribution/	
Availability Codes	
Dist	Avail and/or Special
A-1	20

## FEEDBACK CONTROL OF KARMAN VORTEX SHEDDING

D. S. Park, D. M. Ladd, and E. Hendricks  
NCCOSC, RDT & E  
San Diego, California

### ABSTRACT

A direct numerical simulation of the Navier-Stokes equations of a feedback controlled cylinder wake flow at the Reynolds number of 60 is presented. The simulation shows that vortex shedding behind a circular cylinder is suppressed to a significant degree by applying a feedback forcing with an appropriate phase via blowing/suction slots located at  $\pm 110^\circ$  from the leading edge. Depending on the phase of the feedback forcing relative to the vortex shedding phase, the shedding of the vortices is either suppressed (stabilized) or further enhanced (destabilized).

### 1 INTRODUCTION

Many flows of engineering interest (e.g. separating flows) produce the phenomena of vortex shedding and the associated structural response. Applications include marine structures, underwater acoustics, civil and wind engineering to name a few. The ability to tailor the wake of a bluff body could be used to reduce drag, increase mixing or heat transfer and enhanced combustion. Vortex shedding from bluff bodies has been reviewed most recently by Sarpkaya (1979) and Bearman (1984). Vortex shedding from a cylinder occurs over wide range of Reynolds number from  $47 < Re < 300,000$  and then again at  $Re > 10^6$ . When Reynolds number exceeds a critical value of approximately 47, a symmetry breaking supercritical Hopf bifurcation occurs leading to a discrete frequency vortex shedding known as Karman vortices. Chomaz et al. (1988) have demonstrated that this symmetry breaking Hopf bifurcation is related to the destabilization of a global mode. The existence of an unstable global mode is intimately linked to the fact that the near wake is absolutely unstable followed by the convectively unstable far wake. The understanding of the dynamics of two-dimensional wakes at Reynolds numbers in the vicinity of the critical value is quite firmly established. The preceding description of the vortex shedding mechanism is from an instability perspective. From a mech-

anistic point of view, a flow-induced feedback causes the shedding of the vortices, where the changing location of boundary layer separation on one side of the cylinder causes a change in pressure distribution that forces an opposite asymmetric change in boundary separation. Any small flow perturbation is enough to cause the initial asymmetry that starts the feedback mechanism. The observation that the vortex shedding is caused by the moving location of boundary layer separation is supported by the absence of a distinct shedding frequency in the range  $300,000 < Re < 3,000,000$  where laminar separation followed by turbulent reattachment fixes the turbulent separation location so firmly that feedback is inhibited.

Under the influence of vortex shedding, the changing pressure distribution causes large oscillatory lift forces. When a circular cylinder is flexible and lightly damped or rigid and flexibly mounted, vortex shedding can cause a coupled fluid structure interaction. This flow-induced resonance, causes the body and the wake to oscillate at the same frequency. This phenomenon, alternately called galloping, lock-on or phase locking, results in spanwise phase locking of the fluid and the structure causing coherent vortex shedding along the span of the cylinder.

The important aspect of this phenomenon, from a control standpoint, is that the large pressure forces, both lift and drag, are a result of the small viscous forces acting in the boundary layer of the cylinder. This implies that small control forces applied to the boundary layer can be used to control the larger pressure forces to achieve the effect of modifying the vortex generation and unsteady lift forces. This concept has been demonstrated by Ffowcs Williams & Zhao (1989), where the feedback from a downstream hot film sensor was used to drive a speaker embedded in the wind tunnel wall and suppress vortex shedding from a cylinder in crossflow. The acoustic velocity perturbations from the speaker are many times smaller than the freestream velocity, and yet control was obtained. This study shows that vortex shedding control is a real possibility. Two recent studies (Tokomaru & Dimotakis (1991); Filler et al. (1991)) have shown that small rotation oscillations of a circular cylinder can cause

lock-on. Numerical simulation of Karniadakis & Triantafyllou (1989) have shown that small variations of the near wake produce lock-on.

The emphasis in this work is on active feedback control, as opposed to open loop controls as described in Wu et al. (1989), Tokumaru & Dimotakis (1991), and Filler et al. (1991). In these studies, rotary oscillation of the cylinder was used to alter the cylinder wake, with no feedback from the cylinder or the flow. Open loop control can cause lock-on of vortex shedding and, therefore, modify the vortex shedding phase, but it is highly unlikely that it can suppress the vortex shedding altogether.

The most powerful asymmetric actuator for control of the boundary layer of the flow over a 2-D cylinder is the rotary oscillation of the cylinder wall itself (see Chang (1976) for numerous separation control schemes). However, this method of boundary layer control has certain practical problems in implementation as well as lack of generality to other geometries and therefore will not be considered in this paper.

The next most powerful actuator appears to be a pair of suction/blowing slots located opposite to each other at some location from the leading edge or the stagnation point. A small amount of fluid sucked in one slot, thinning the boundary layer, and ejected out through the other slot, will asymmetrically change the location of the boundary layer separation.

In this paper, we will consider the problem of suppressing or stabilizing the near wake of a flow past a circular cylinder at low Reynolds number by direct numerical simulation of 2-D Navier-Stokes equations.

## 2 NUMERICAL PROCEDURE

The control problem is investigated by numerically solving the 2-D Navier-Stokes equations in a stream function/vorticity formulation as follows;

$$\frac{\partial \omega}{\partial t} + \nabla \cdot (\psi \omega) = \frac{2}{Re} \nabla^2 \omega, \quad (1)$$

$$\nabla^2 \psi = -\omega, \quad (2)$$

where  $\omega$  and  $\psi$  are the vorticity and the stream function, respectively. The above equations are nondimensionalized using the cylinder radius,  $R$ , the freestream velocity,  $U$ , and the kinematic viscosity of the fluid,  $\nu$ . The Reynolds number  $Re$  is defined as follows;

$$Re = \frac{Ud}{\nu}, \quad (3)$$

where  $d$  is the cylinder diameter. The boundary conditions on the cylinder surface are

$$\frac{\partial \psi}{\partial r}(r=1, \theta, t) = 0, \quad (4)$$

$$\psi(r=1, \theta, t) = \psi_w(\theta, t). \quad (5)$$

In the case of zero blowing/suction,  $\psi_w(\theta, t)$  is identically equal to zero. Here we have two boundary conditions for the stream function while there is no boundary condition for the vorticity. Therefore, the second order accurate boundary condition for the vorticity at the cylinder surface is derived using equation (2) and the boundary conditions for the stream function. The outer boundary conditions are

$$\psi_\infty = Uy - \frac{F_0}{2\pi} \ln(r) + \frac{1}{2\pi} \sum_{n=1}^{\infty} \frac{1}{n} \{F_n \cos(n\theta) + G_n \sin(n\theta)\} r^{-n}, \quad (6)$$

$$\omega_\infty = 0. \quad (7)$$

The readers are referred to Sa and Chang (1990) for the definitions and the derivations of  $F_n$  and  $G_n$ .

The equations (1) and (2) are discretized by a second order central differencing in radial direction and a pseudo spectral method is used in the circumferential direction. The temporal advancement is done via two fractional steps (Korezjak & Patera (1986)). The first step is the nonlinear explicit step to compute the effect of the nonlinear advective term as follows;

$$\frac{\omega^* - \omega^n}{\Delta t} = \sum_{q=0}^2 \beta_q \nabla \cdot (\psi^{n-q} \omega^{n-q}), \quad (8)$$

where  $\beta_0 = 23/12$ ,  $\beta_1 = -16/12$ , and  $\beta_2 = 5/12$ , and  $\omega^*$ ,  $\omega^n$  and  $\psi^n$  denote the intermediate vorticity, the vorticity and the stream function at  $n$ -th time level, respectively. The second step is the implicit step, where the viscous effect is computed as follows;

$$\frac{\omega^{n+1} - \omega^*}{\Delta t} = \frac{2}{Re} \nabla^2 \frac{\omega^{n+1} + \omega^*}{2}. \quad (9)$$

After the vorticity at  $(n+1)$ -th time level,  $\omega^{n+1}$ , is computed, the stream function,  $\psi^{n+1}$ , is obtained by solving the equation (2)

for the stream function. The accuracy of the numerical scheme is second order in both space and time.

The computational grid is uniformly stretched in radial direction such that the grid is denser near the cylinder surface to resolve the high gradient of the flow there. A typical grid is shown in figure 1. The outer computational boundary is located at  $r_\infty = 59.38$ . The number of grid points in circumferential and radial directions are 256 and 128, respectively.

## 3 RESULTS AND DISCUSSION

Accuracy of numerical method was validated by comparing the numerically obtained Strouhal number ( $St$ ) to the experimental values at the Reynolds numbers of 60, 100, 150 and 200. The nondimensional frequency  $St$  is defined as  $f_d d/U$ , where  $f_d$  is the frequency of vortex shedding. In experiments at these Reynolds numbers, due to the finite aspect ratio effect of the cylinder, the vortices are shed from the cylinder at a small oblique angle to the cylinder. Williamson (1989) found that the  $St - Re$  discontinuities occurring at low Reynolds numbers are due to the obliqueness of the vortex shedding. He noticed that the parallel shedding and the oblique shedding are related by the cosine of the angle as follows. The frequency of the parallel shedding can be obtained by dividing the frequency of the oblique shedding by the cosine of the angle of the shedding that is the angle between the spanwise oblique vortex line and the cylinder axis. He also presented the universal  $St - Re$  curve without discontinuities by correcting the effect of the obliqueness of the vortex shedding. Our results are plotted with these corrected experimental values of Williamson (1989) in figure 2. The agreement is excellent. The results will presented for the case of the Reynolds number of 60.

The lift coefficient is evaluated directly from the known vorticity field by the following formula

$$C_L = \frac{2}{Re} \int_0^{2\pi} \left( \omega - \frac{\partial \omega}{\partial r} + \frac{3}{\pi} \frac{du_w}{d\theta} \right)_{r=1} \cos(\theta) d\theta, \quad (10)$$

where  $u_w$  is the radial velocity at the cylinder surface due to the radial blowing/suction velocity through the blowing/suction slots. The first term is the contribution to the lift of the tangential viscous force and the second term is the lift due to the pressure force. The pressure force is the dominant term in equation (10). In particular,  $C_L$  is positive in the positive  $y$ -direction.

The location of the actuator or the blowing/suction slots is a critical factor in their effectiveness for the suppression of the vortex shedding. We have tried the blowing/suction slots at  $\pm 50^\circ$ ,  $\pm 65^\circ$ , and  $\pm 110^\circ$  from the leading edge of the cylinder. With the actuators at  $\pm 50^\circ$ , or  $\pm 65^\circ$ , suppression of the vortex shedding was not obtained. We think the ineffectiveness of the actuator was due to the fact that the actuator was located too far from the separation point on the cylinder surface. The separation points on the cylinder surface, at the Reynolds number of 60, wander around  $\pm 120^\circ$  as the vortices are shed. When the blowing/suction slots were located at  $\pm 110^\circ$  from the stagnation point, that is slightly ahead of the separation points of the unforced wake, they proved to be strong actuators.

The blowing/suction velocity through small slots is dictated according to the following feedback law.

$$u_f = \alpha \frac{\omega(x_s, y = 0)}{\omega_{max}}, \quad (11)$$

where  $\alpha$  is the feedback coefficient,  $\omega(x_s, y = 0)$  is the measured vorticity at the downstream location,  $x_s$ , along the centerline and  $\omega_{max}$  is the maximum vorticity at the same spatial location for the unforced wake. Here, positive  $u_f$  denotes blowing/sucking through upper/lower slots. This choice of the feedback law is motivated by the fact that as the flow becomes controlled and approaches the symmetric configuration, the vorticity  $\omega(x_s, y = 0)$  tends to zero resulting in the small amount of feedback. Therefore, as the desired state is approached, the required forcing level becomes small.

The phase relation of the feedback relative to the vortex shedding phase was determined by the downstream location of the feedback "sensor",  $x_s$ . To properly choose  $x_s$ , the movement of the separation point as the vortices are shed must be known. Figure 3 is the temporal plot of the vorticity at 6.01 radius downstream ( $x = -6.01$ ) along the centerline ( $y = 0$ ) and the vorticity at cylinder surface ( $r = 1$ ) at an angle of  $110^\circ$ , which is slightly ahead of the upper separation point for the unforced wake. The vorticity measured on the centerline oscillates around zero mean while the vorticity near the separation point oscillates around some mean value. Let us denote  $\omega_c$  and  $\omega_s$  to be the vorticity at the centerline and the vorticity on the cylinder surface, respectively. The phase relation between these two are as follows;

$$\omega_c = A \sin(2\pi f t), \quad (12)$$

$$\omega_s = B \sin(2\pi f t + \phi) + \omega_{mean}, \quad (13)$$

where  $\phi$  is computed to be  $-0.7117\pi$ . The nondimensional frequency,  $f$ , is the half of the Strouhal number,  $St$ . Feeding back the phase of the vorticity at  $110^\circ$  was tried first. The appropriate sensor location,  $x_s$ , for this phase is approximately 8 to 9 radius downstream. The feedback coefficient  $\alpha$  was varied from 0.3 to 1.8 for the fixed sensor location at 8.5 radius downstream. Sup-

pression of the vortex shedding was obtained although it was not total suppression. Figure 4 shows the vorticity plots for several  $\alpha$ 's. The optimum value for  $\alpha$  appears to be close to 1.1. As  $\alpha$  increases from a small value, the vortex shedding becomes slightly suppressed, with maximum suppression occurring at 1.1. As  $\alpha$  becomes larger than 1.1, the vortex shedding is enhanced. For  $\alpha = 1.1$ , the near wake structure looks almost symmetrical. Figure 5 are the corresponding streamline plots. For the optimum value of  $\alpha$ , the recirculating zone is elongated approaching the steady solution. According to the calculation of Eouberg (1980) of steady flow past a circular cylinder at  $Re = 60$ , the length of the recirculating wake bubble is around 4 cylinder diameters. When the shedding is nearly suppressed, the recirculating wake bubble is approximately 3 to 4 cylinder diameter long.

Next, we fixed the feedback coefficient  $\alpha$  at 1.1 and varied the sensor location. The suppression of vortex shedding was obtained only at narrow range of the sensor location, which is from 7.5 radius downstream to 9 radius downstream. The optimum sensor location is around 8 radius downstream. In figure 6, the vorticity plots for the flows with the sensors located at various locations are given. The corresponding streamline plots are shown in figure 7. With the sensor located at two radius downstream, the vortex shedding process is enhanced instead of being suppressed as shown in figure 6a. As the forcing is turned on, the vorticity and velocity fluctuations increase by about 100% within one vortex shedding period. Ffowcs Williams & Zhao (1989) also observed that the phase reversal of the loud speaker from the controlled case brought about an enhancement of the fluctuation. Let us take a look at the optimum case, which is the flow with the feedback sensor located at 4 diameters downstream. The near wake vorticity plot in figure 6b looks almost symmetric. The streamline plot in figure 7b shows the recirculating wake bubble of the length of approximately 4 cylinder diameters. Figure 8 and 9 are the time series of the lift coefficient and the streamwise velocity at one diameter downstream and one radius above the centerline, respectively. Forcing is turned on at  $t = 34$  and is turned off at  $t = 500$ . As the forcing is turned on, the fluctuations decay rapidly to a low level. The lift coefficient fluctuation amplitude and the velocity fluctuation amplitude are reduced to 25% and 15% of the unforced case, respectively. The mean of the fluctuating velocity has also decreased. As forcing is turned on, the cylinder wake slowly returns to the natural vortex shedding state as also observed by Ffowcs Williams & Zhao (1989). Figure 10 is the time series plot of the square of the lift coefficient on a semi-log scale. As forcing is turned off, the fluctuation begins to increase exponentially as demonstrated by the straight line on a semi-log plot. This region is called a linear growth region which is followed by a transition region and a saturation state as also observed in the numerical simulation by Hannemann & Oertel (1989). When the forcing is on, the fluctuations modulate. The modulations of the fluctuations can be explained as follows. As the forcing becomes small, the suppression of the vortex shedding relaxes slightly resulting in the increased vorticity fluctuation. This increases the forcing level once again. The increased forcing suppresses the vortex shedding process. Then the forcing decreases again.

Lastly, we briefly look at the downstream development of the vortical structures. Figure 11 shows the vortical development of the wakes of the unforced case and that of the suppressed case up to 27 diameters downstream. Although the near wake is suppressed to a significant degree, the small fluctuation in the near

wake becomes amplified due to the convective nature of the instability of the far wake as the fluctuation travels downstream. This is also observed by Ffowcs Williams & Zhao (1989) and shown in figure 5 of these authors. Despite of the fact that the near wake spectral level is low since the wake is controlled, the spectral level increases exponentially in the downstream direction.

#### 4 CONCLUSION

We have been able to suppress the vortex shedding behind a circular cylinder in a two dimensional numerical simulation at the Reynolds number of 60 by active feedback control method. The actuators we chose to use were the blowing/suction slots located at  $\pm 110^\circ$  from the leading edge of the cylinder. The control was possible in only a narrow range of phase while the vortex shedding was enhanced if forced with the phase out of this range. Although the present results are for the Reynolds number of 60, a quite low Reynolds number, the authors believe that this active feedback control will still be operative even at higher Reynolds numbers. The higher Reynolds number flow control is currently being studied. One of us (D. S. Park) thanks the support of the ONT (Office of Naval Technology) Postdoctoral Fellowship.

#### REFERENCES

Bearman, P.W., 1984, "Vortex Shedding from Oscillating Bluff Bodies", *Ann. Rev. Fluid Mech.*, Vol. 16, 195-222.

Chang, P.K., *Control of Flow Separation*, Hemisphere Pub. Co. 1976.

Chomaz, J.M., Huerre, P. and Redekopp, L.T., 1988, "Bifurcations to Local and Global Modes in Spatially Developing Flows", *Phys. Rev. Lett.*, Vol. 60, 25-28.

Ffowcs Williams, J.E. and Zhao, B.C., 1989, "Active Control of Vortex Shedding", *J. of Fluids and Structures* 3, 115-122.

Filler, J.R., Marston, P.L. and Mih, W.C., 1991, "Response of the Shear Layers Separating from a Circular Cylinder to Small Amplitude Rotational Oscillations", *J. Fluid Mech.*, Vol. 231, 481-499.

Fornberg, B., 1980, "A numerical study of steady viscous flow past a circular cylinder", *J. Fluid Mech.*, Vol. 98, 819-855.

Hannemann, K. and Oertel Jr, H. 1989 "Numerical Simulation of the Absolutely and Convectively Unstable Wake", *J. Fluid Mech.*, Vol. 199, 55-88.

Karniadakis, G.E. and Triantafyllou, G.S., 1989, "Frequency Selection and Asymptotic States in Laminar Wakes", *J. Fluid Mech.*, vol 199, 441-469.

Korczak, K.Z. and Patera, A.T. 1986, "An Isoparametric Spectral Element Method for Solution of the Navier-Stokes Equations in Complex Geometry", *J. Comp. Physics*, 62, 361-382.

Sa, J.Y. and Chang, K.S., 1990, "On Far Field Stream Function Condition for Two-Dimensional Incompressible Flows", *J. Comp. Physics*, 91, 398-412.

Sarpkaya, T., 1979, "Vortex Induced Oscillations: A Selective Review", *J. Appl. Mech.*, Vol. 46, 241-258.

Tokamaru, P.T. and Dimotakis, P.E., 1991, "Rotary Oscillation Control of a Cylinder Wake", *J. Fluid Mech.*, Vol. 221, 77-90.

Williamson, C.H.K., 1989, "Oblique and Parallel Modes of Vortex Shedding in the Wake of a Circular Cylinder at Low Reynolds Numbers", *J. Fluid Mech.* 206, 579-627.

Wu, J., Mo, J. and Vakili, A., 1989, "On the Wake of a Cylinder with Rotational Oscillations", *AIAA-89-1024*.

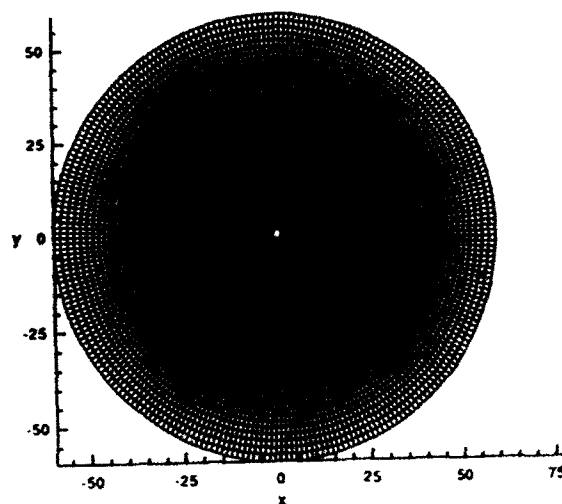


Figure 1: Computational grid; 256 x 128.

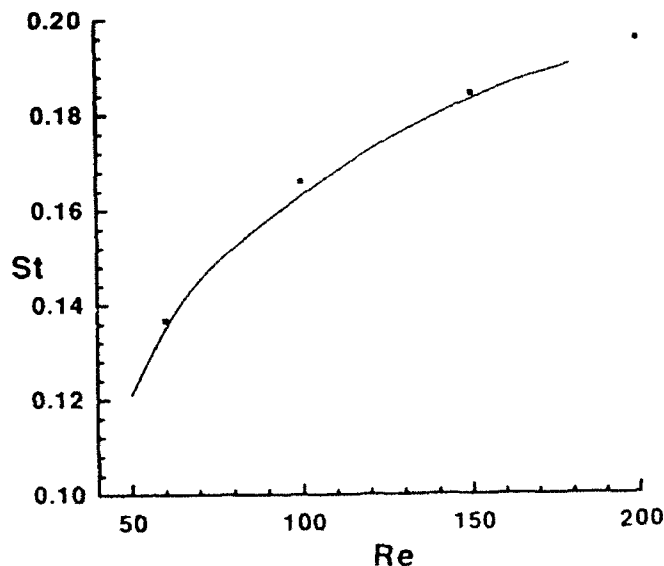


Figure 2:  $St$  versus  $Re$ ; solid line is data from Williamson (1989) and solid square is the present data

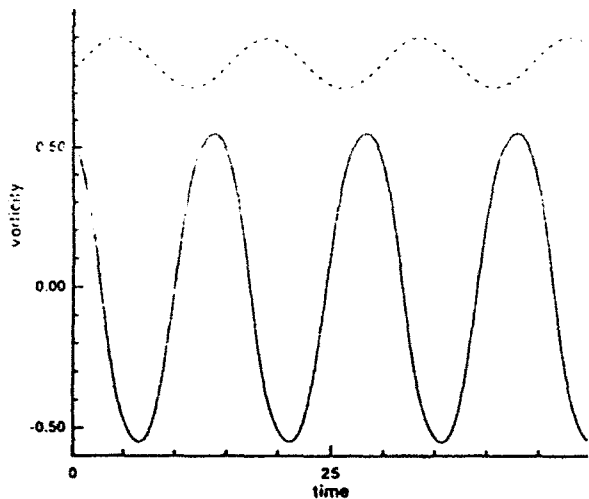


Figure 3: Vorticity time series (solid line;  $x = -6.01, y = 0$ . dashed line;  $r = 1, \theta = 110^\circ$ ).

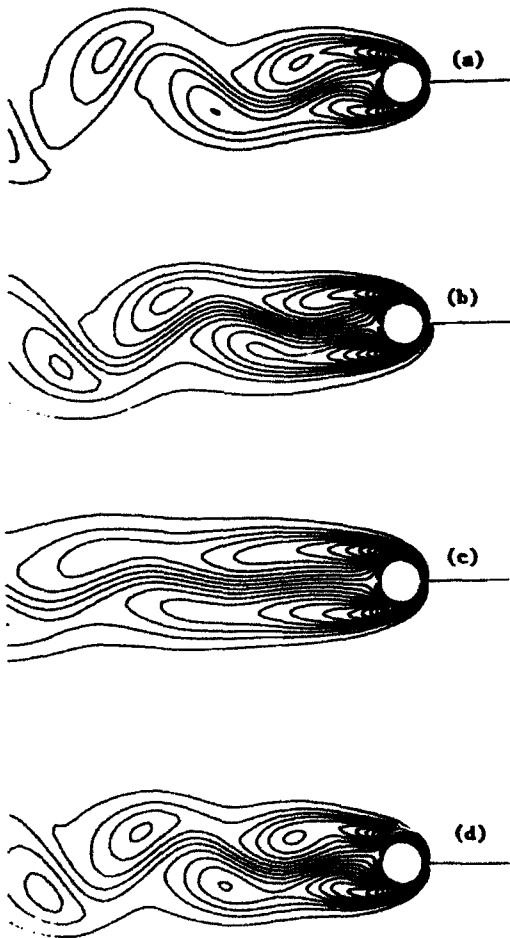


Figure 4: Vorticity contour for the sensor ( $x_s$ ) located at 8.5 radius downstream ( $x_s = -8.5$ ). Flow is from right to left. a)  $\alpha = 0$  (natural shedding), b)  $\alpha = 0.3$ , c)  $\alpha = 1.1$ , d)  $\alpha = 1.8$ .

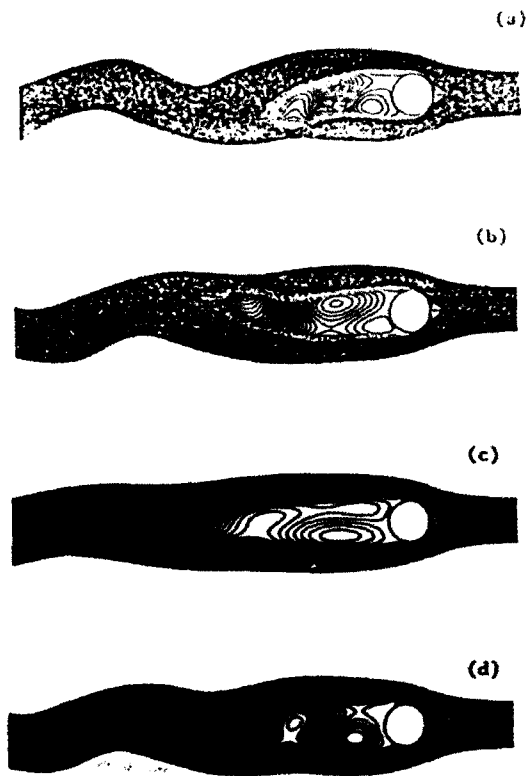


Figure 5: Streamline plot for the sensor ( $x_s$ ) located at 8.5 radius downstream ( $x_s = -8.5$ ). a)  $\alpha = 0$  (natural shedding), b)  $\alpha = 0.3$ , c)  $\alpha = 1.1$ , d)  $\alpha = 1.8$ .

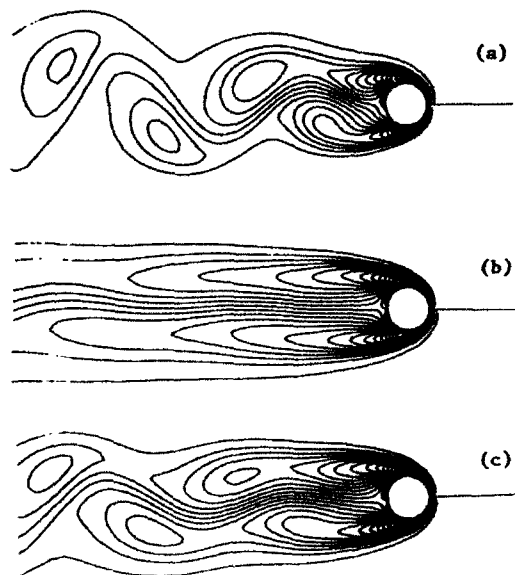


Figure 6: Vorticity contour for  $\alpha = 1.1$ . a)  $x_s = -2$ , b)  $x_s = -8$ , c)  $x_s = -9$ .

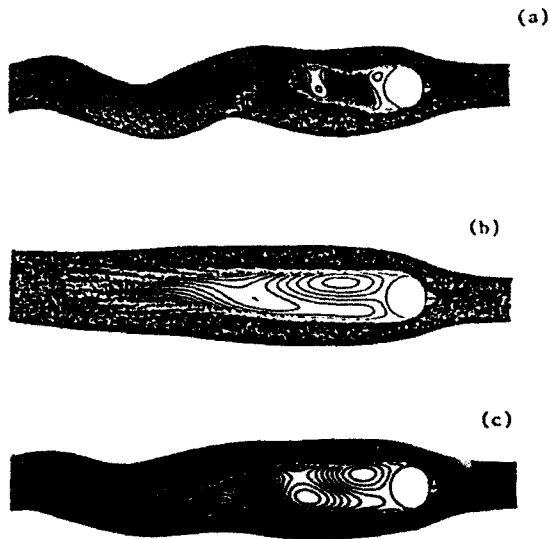


Figure 7: Streamline plot for  $\alpha = 1.1$ . a)  $x_s = -2$ , b)  $x_s = -8$ , c)  $x_s = -9$ .

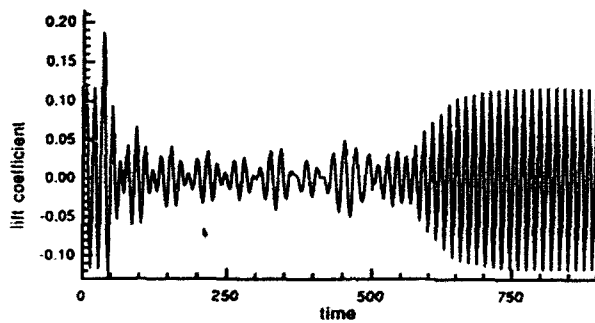


Figure 8: Plot of time series of lift coefficient for  $\alpha = 1.1$  and  $x_s = -8$ . Forcing is turned on at  $t = 34$  and turned off at  $t = 500$ .

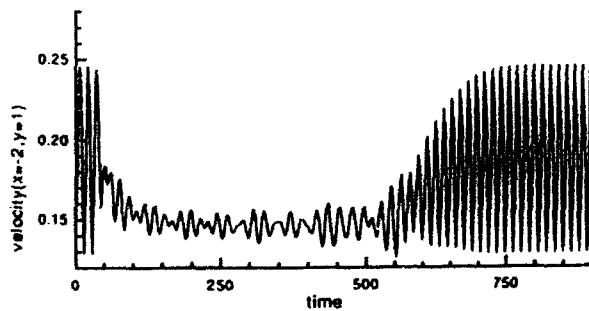


Figure 9: Plot of time series of Streamwise velocity at  $x = -2$  and  $y = 1$  for  $\alpha = 1.1$  and  $x_s = -8$ . Forcing is turned on at  $t = 34$  and turned off at  $t = 500$ .

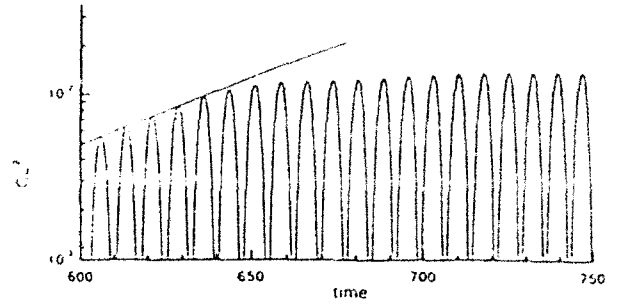


Figure 10: Semi-log plot of time series of the square of lift coefficient for  $\alpha = 1.1$  and  $x_s = 8$ . The response after forcing is turned off is shown.

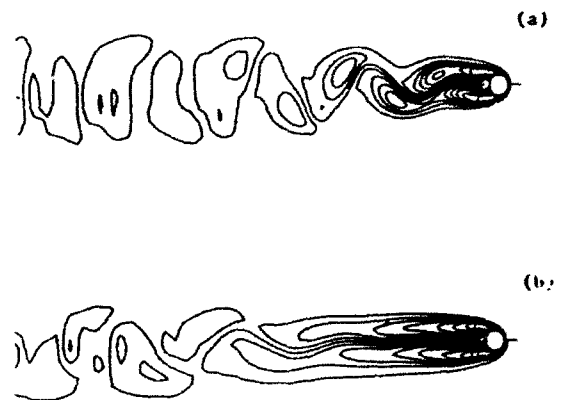


Figure 11: Downstream development of vorticity. a) natural shedding, b) suppressed shedding ( $\alpha = 1.1$ ,  $x_s = -8$ ).